A Simplified Quasi-Linear Model for Wave Generation and Air–Sea Momentum Flux

ALASTAIR D. JENKINS

The IBM Bergen Environmental Sciences and Solutions Centre, Bergen, Norway

(Manuscript received 21 January 1992, in final form 3 March 1993)

ABSTRACT

A simplified model is described for wave generation and air–sea momentum flux. The model is based upon the quasilinear theory employed by Fabrikant and Janssen, in which the mean flow is approximated to second order in the wave amplitude and fluctuating quantities are approximated to first order. The wave generation rate is computed using Miles' wave generation theory and the numerical method of Conte and Miles.

The computationally expensive iterative procedure used in Janssen's quasi-linear model is avoided by specifying in advance the vertical wind velocity profile as a combination of a logarithmic profile above height $z = z_p$ and a square root profile below that height, z_p being given by $U(z_p) = c(k_p)$, where U is the wind velocity, k_p is the wavenumber at the peak of the wave spectrum, and $c(k_p)$ is the associated phase speed. In contrast to Janssen's model and his subsequent simple surface-layer model, no explicit surface roughness parameter is specified: the whole of the applied wind stress is assumed to be taken up by waves with the simple one-dimensional energy spectrum $E(k) = (1/2)\alpha_P k^{-3}$ for wavenumbers k between k_p and ∞, $E(k) = 0$ for $k < k_p$. The square root part of the velocity profile is derived by assuming that the form of the sea surface is stochastically self-similar, and that the velocity profile is also self-similar. A self-similar velocity profile requires $kz_c(k)$ to be independent of k, where $U[z_c(k)] = c(k)$.

The model gives a rather crude approximation to the wave generation rate. The quantity $\sigma^{-1}\dot{E}_{in}(k)/E(k)$, where σ is the wave angular frequency and $\dot{E}_{in}(k)$ is the rate of wave energy input, is independent of k for a spectrum of the form $E(k) \propto k^{-3}$. It is proportional to $(U_*/c_p)^2$ if the Phillips parameter α_P is constant and to $(U_*/c_p)^{1/2}$ if $\alpha_P \propto (c_p/U_*)^{-3/2}$, where U_* is the friction velocity and $c_p = c(k_p)$.

Air–sea momentum flux, as described by the drag coefficient $C_D(10\text{ m}) = [U_*/U(10\text{ m})]^2$, is represented rather better. For wave age c_p/U_* above 5–10 it decreases with increasing wave age if U_* is kept constant. The predicted drag coefficient, however, tends to decrease more rapidly with wave age for the older wind seas than field measurements indicate [if we assume $\alpha_P \propto (c_p/U_*)^{-3/2}$]. For very young seas with $c_p/U_* < 5$, the drag coefficient increases with wave age. The model predicts a significant variation of drag coefficient with wave age even when α_P is constant. For sea states so "old" that $z_p > 10$ m, the wind speed depends just on c_p/U_*, and $C_D(10\text{ m})$ increases again with wave age. This last, counterintuitive situation will be modified if we allow more of the air–sea momentum flux to be supported directly by turbulence.

1. Introduction

The resonant interaction of gravity waves with a plane-parallel flow according to the theory of Miles (1957) is a commonly accepted mechanism for the generation of waves by wind. Resonance occurs at a so-called "critical level"—at a height $z = z_c$ where the wind speed $U(z_c)$ is equal to the phase speed c of the waves. [If the wind direction is at an angle θ to the direction of wave propagation, the resonance condition becomes $U(z_c)\cos\theta = c$.] If the curvature of the wind velocity profile,

$$\kappa_U \equiv \frac{d^2U/dz^2}{(dU/dz)^3}, \tag{1}$$

is negative at $z = z_c$, the resonance process will induce air pressure fluctuations at the water surface with a component in phase with the surface slope, which will transfer energy into the waves and tend to make them grow, by the mechanism of Jeffreys (1925). For random waves with a continuous spectrum, the wave–mean flow resonance will occur over a range of critical levels, corresponding to the range of phase speeds of the Fourier components of the wave field.

a. Consistent treatment of wave generation and momentum flux

The Miles (1957) theory is linear, in that the surface pressure fluctuations, and thus the wind-to-wave energy flux, are directly proportional to the wave amplitude. Waves of finite amplitude a are associated with a momentum proportional to a^2. If wave–mean flow resonant interaction transfers energy from the wind to the waves, it must also transfer momentum; Stewart (1961, 1974) pointed out that this was very likely to affect the

Corresponding author address: Dr. Alastair D. Jenkins, The IBM Bergen Environmental Sciences and Solutions Centre, Thormøhlensgate 55, N-5008 Bergen, Norway.

wind velocity profile. Thus, the air–sea momentum flux, and consequently the effective drag coefficient, will depend on the wave conditions, as observed by Donelan (1982).

A consistent theory of the two-way interaction between the wave field and the wind profile must be nonlinear, so that it takes account of the $O(a^2)$ wave momentum. Fabrikant (1976) presented such a consistent theory, making use of the mathematical similarity between the Miles (1957) wave–mean flow resonant interaction and Landau's (1946) theory of the interaction of plasma waves and charged particles. Fabrikant's presentation assumes that a random phase approximation can be used to describe the wave field, and uses the quasi-linear approximation, in which $O(a)$ and average $O(a^2)$ quantities are taken into account, but fluctuating $O(a^2)$ and higher-order quantities are neglected. His basic result is that the wind velocity obeys a nonlinear diffusion-type equation (neglecting viscosity and turbulent Reynolds stresses):

$$\frac{\partial U}{\partial t} = D(z, U)\frac{\partial^2 U}{\partial z^2}. \qquad (2)$$

The wave diffusion coefficient D at a height z is proportional to the squared modulus of the Fourier coefficient $\chi_k(z)$, at wavenumber k, of the velocity streamfunction (or of the vertical velocity component), where k is given by $c(k) = U(z)$, assuming for simplicity that the waves are unidirectional. The streamfunction Fourier coefficient is in turn found by solving the Rayleigh equation, which appears in the Miles (1957) wave generation theory:

$$[U - c(k)]\left(\frac{d^2\chi_k}{dz^2} - k^2\chi_k\right) - \frac{\partial^2 U}{\partial z^2}\chi_k = 0. \qquad (3)$$

For time $t \to \infty$, the velocity profile tends to a linear profile for heights z where the value of the wave energy spectrum $E(k)$, with k given by $c(k) = U(z)$, is greater than zero. Since the curvature κ_U is then zero, there will then be zero energy flux from the wind to the waves.

Janssen (1982) derived (2) using multiple time scale analysis. For the inviscid stationary state, where the wind velocity profile is linear, he found that the wave energy spectrum $E(\sigma)$ became proportional to σ^{-4} for deep-water gravity waves with dispersion relation $\sigma^2 = gk$, where σ is the wave angular frequency, and g is the acceleration due to gravity. This corresponds to a spectrum in terms of scalar wavenumber, $E(k) \propto k^{-5/2}$.

Janssen (1989) added viscosity and a Prandtl mixing length turbulent Reynolds stress term to the diffusion equation (2) in order to calculate wave generation rates and wave-induced drag coefficients over a sea surface with JONSWAP-type (Joint North Sea Wave Project) wave spectra. If the time derivative term is neglected, (2) can then be written as

$$\frac{d}{dz}\left(\rho\nu\frac{dU}{dz} + \tau_t(z) + \tau_w(z)\right) = 0, \qquad (4)$$

where ν is the kinematic molecular viscosity of air, ρ is the air density, $\tau_t = \rho(\kappa z)^2|dU/dz|dU/dz$ is the turbulent Reynolds stress, $\kappa \approx 0.4$ is von Kármán's constant, and $\tau_w(z) = -\int_z^\infty dz' D(z', U)d^2U/dz'^2$ can be termed the "wave stress." Janssen (1989) solved iteratively by finite differences a coupled system of 26 ordinary differential equations—Eq. (4) plus a Rayleigh equation of the form (3) for each of 25 wave Fourier components. The computation was expensive: it was necessary to use 10 000 grid points for (4) in order to calculate d^2U/dz^2 sufficiently accurately. For the purpose of incorporating the effect of ocean waves in numerical atmospheric models, Janssen and his colleagues later employed simplified parameterizations (Janssen et al. 1989; Janssen 1991). The parameterization employed by Janssen (1991) assumed that although the waves affected the wind velocity profile, the shape of the profile remained logarithmic.

Jenkins (1992) produced a quasi-linear model that took account of viscosity and air turbulence in the wind–wave interaction equations as well as the diffusion equation. The critical level for resonant interaction of each Fourier component was then effectively replaced by a broader zone, and only 100 grid points were required for reasonable accuracy. The complicated nature of the model equations resulted in slow convergence (typically, 1000 iterations were required).

A more direct approach to the wind–wave interaction problem is to solve the fully nonlinear hydrodynamic equations directly over a time-varying ocean surface, using a suitable turbulence closure scheme to account for subgrid-scale motions. This was performed for simulated continuous wave spectra by Chalikov (1978, 1986a,b), Makin (1980, 1982, 1987), and Makin and Panchenko (1986): the great computational expense of such a model is obvious. Chalikov and Makin (1991) also presented a simplified model of wind–wave interaction, based on the results of their previous computations. They assumed that the wind velocity profile was composed of two pieces, both logarithmic in form, with a discontinuity in the velocity gradient at a level that depended on the dominant wavelength of the surface waves.

b. *Surface roughness*

The models of Chalikov, Makin and Panchenko, Janssen (1989), and Jenkins (1992), which take account of atmospheric turbulence, all employ a surface roughness parameter z_r. In the absence of waves and neglecting molecular viscosity, these models produce a logarithmic wind velocity profile,

$$U(z) = \frac{U_*}{\kappa}\log\frac{z}{z_r}, \qquad (5)$$

where $\kappa \approx 0.4$ is von Kármán's constant, $U_* = [\tau_t(\infty)/\rho]^{1/2}$ is the friction velocity, and z_r is equal to the aerodynamic roughness length z_0 under these conditions. For neutrally stratified turbulent flow over a solid boundary, the roughness length is found to be proportional to ν/U_* if the boundary is smooth, and it is more or less proportional to the size of the roughness elements if the boundary is rough. For a water surface, the situation is more complex, because the capillary and gravity waves, which can form the roughness elements, are moving and are also influenced by the air motions. Nevertheless, if the velocity profile is approximately logarithmic, it is possible to determine z_0 by curve fitting.

There is a diversity of opinion in the literature about how to describe the aerodynamic roughness of the sea surface, and on the equivalent question of what types of surface irregularity support the air–sea flux of momentum. The alternatives can be (i) the momentum flux is supported by flow separation from short waves in which capillary forces are important, in a narrow band of wavelengths, (ii) the momentum flux is supported by a wide band of wavelengths, for the most part long gravity waves in which capillarity is insignificant, (iii) it is supported by flow separation from relatively long gravity waves with a narrow band of wavelengths, or (iv) the sea surface is aerodynamically smooth, with roughness length of order ν/U_*.

Alternative (i), that momentum flux is supported by short waves with a well-defined wavelength, is argued for by Csanady (1985, 1990), based on laboratory observations of flow separation above waves and of large fluctuations in shear stress at the water surface (Okuda et al. 1977; Kawai 1981, 1982). Csanady's mechanism is associated with a balance between energy input to the wavelets by a fluctuating shear stress correlated with the wave orbital velocity, and wave dissipation by vortical motions (turbulence or wave breaking). This mechanism can in fact be scaled up to longer gravity waves, so that we approach alternative (iii), suggested by Stewart (1974), where most of the momentum flux is supported by the dominant wave component of the sea state, as deduced by Hsu et al. (1982) from laboratory measurements by Wu et al. (1979) combined with a nonlinear theoretical model developed by Yuen and Lake (1979). This is supported by the laboratory experiments of Banner (1990a) on airflow and pressure fluctuations over breaking and almost-breaking gravity waves, where the correlation between pressure and the surface slope of the wave accounts for between 0.75 and 0.86 of the total momentum flux. Of course the balance of the momentum flux will have to be taken up by shear stress fluctuations at the dominant wave scale, by shorter waves, or by a laminar boundary layer, of which the last two contributions can be described by a roughness parameter z_r.

We should be cautious in interpreting the results of laboratory experiments as being representative of conditions over the real ocean. The laboratory experiments quoted here are for rapidly growing waves with a nondimensional wave age c_p/U_* in the range 0.3–2, where c_p is the phase speed of the dominant wave component. Field measurements for wind waves in the open ocean give values of c_p/U_* that are usually between 7 and 25, so there is virtually no overlap in this parameter. Field and laboratory measurements will thus be for waves of quite different shapes, since wave steepness decreases with wave age. Also, the small scales of laboratory experiments mean that the effects of surface tension and molecular viscosity will be more noticeable.

Some authors have modeled the airflow over waves using a z_r that is allowed to vary during the wave cycle, being generally greater at the wave crests than in the troughs (Al-Zanaidi and Hui 1984; Chalikov 1986b; Chalikov and Makin 1991; Maat and Makin 1992). This behavior is inherent in the turbulence closure techniques used by these authors, and appears to give good results when modeling flows over breaking waves.

Banner's (1990a) experiment was with waves of fixed form running against a water current. In the field, the wave spectrum will be much broader and the surface will not be stationary in any reference frame. His experimental results would also be consistent with alternative (ii), where the momentum flux is supported by a broad spectrum of waves. Donelan (1990, p. 267) has commented, "Field experiments ... have so far managed to explore [the momentum flux to wave components in] only the region near the peak [of the spectrum]." Many authors have supported the idea that momentum flux is supported by both long and short waves (e.g., Stewart 1961; Kitaigorodskii 1973; Donelan 1982; Wu 1986; Janssen 1989; Nordeng 1991; Jenkins 1992; Chalikov and Belevich 1993). Usually, a roughness parameter is used to describe the momentum flux to the short-wave part of the spectrum: Kitaigorodskii (1973) and Nordeng (1991) extend its use in a uniform manner to the whole spectrum by allowing the roughness elements of different scales to move with the appropriate phase speed.

If a roughness parameter is used to account for the effect of short waves, a Charnock-type formulation,

$$z_r = \alpha_C U_*^2/g, \tag{6}$$

has been used by, for example, Janssen (1989). Strictly speaking, z_0 should be used rather than z_r in the preceding expression since Charnock (1955) introduced his formulation to account for the behavior of the overall drag coefficient. Janssen (1989) uses Garratt's (1977) value $\alpha_C = gz_0/U_*^2 = 0.0144$, obtained from a review of field observations. However, a later analysis by Wu (1980) gives $\alpha_C = 0.0185$, so Janssen's use of a somewhat lower value to account for the unresolved roughness elements alone may perhaps be justified. In any case, the numerical modeler is faced with a di-

lemma: he or she is required to make a rather arbitrary decision as to how to describe the effect of short waves and other contributions to the total drag not accounted for in the main part of the model.

In the model described in the present article, I treat the whole wave spectrum in a uniform manner. However, instead of assuming that the wave spectral components act as roughness elements in a classical turbulent boundary layer, I assume that they extract an amount of momentum from the mean flow equal to the amount that they require for their own "wave momentum," as they extract energy from the wind by the mechanism postulated by Miles (1957). This is a rather "extreme" treatment of the dilemma described in the previous paragraph: the whole of the momentum flux is assumed to be supported by surface gravity wave generation.

c. *Brief description of simplified model*

As has been indicated in the previous sections, this paper attempts to address two of the problems encountered in the models of Chalikov and Makin (e.g., Chalikov 1986b), Janssen (1989) and Jenkins (1992): (i) computational expense and (ii) the specification of a surface roughness parameter. The roughness parameter problem is dealt with by neglecting surface tension, so that we have pure surface gravity waves, and assuming that the Miles (1957) wave–mean flow resonance mechanism operates to arbitrarily small wavelengths. The wave energy spectrum in the high-frequency tail is assumed to be

$$E(k) = \frac{1}{2}\alpha_P k^{-3}, \tag{7}$$

where the exponent (-3) is consistent with the stereophotographic wave measurements of Banner et al. (1989). This can still be in agreement with a frequency spectrum $E(\sigma) \propto \sigma^{-4}$ if we allow for the Doppler shifting of short waves by the orbital motions of longer waves (Banner 1990b). The Phillips parameter α_P is allowed to vary, depending on wave age c_p/U_*. For simplicity, the waves are assumed to be unidirectional and $E(k)$ is set to zero for wavenumbers less than that of the spectral peak, k_p. Neglecting molecular viscosity, we assume that at the sea surface (now $z = 0$, not $z = z_r$) all the air–sea momentum flux is carried by the wave stress, that is, $\tau_w(0) = \tau_t(\infty) = \rho U_*^2$. Wind–wave resonant interaction will occur at critical levels $\{z_c: 0 < z_c \leqslant z_p\}$, corresponding to $\infty > k \geqslant k_p$. The mechanism described here only takes account of the momentum flux to surface gravity waves. In addition, we assume that the system is in a nearly stationary state: although the wave field can change slowly with time, as energy is fed into it from the wind, we assume that this change is on a much longer time scale than the response time of the atmospheric boundary layer.

The computational expense is reduced by specifying the wind velocity profile in advance, rather than by determining it iteratively. We assume that for all Fourier components of the wave spectrum, the ratio of the critical height to the wavelength is constant, that is, $kz_c(k)$ is constant. For deep-water gravity waves, this means that $U(z) \propto z^{1/2}$ for $z \leqslant z_p$, and that τ_w decreases linearly from ρU_*^2 at $z = 0$ to zero at $z = z_p$. Equation (4) is satisfied by letting τ_t increase linearly from zero at $z = 0$ to ρU_*^2 at $z = z_p$, becoming constant for $z \geqslant z_p$. For the purpose of solving the Rayleigh equation (3), the square root profile of $U(z)$ is assumed to extend to $z \to \infty$, whereby it suffices to solve (3) for a single Fourier component only, the solutions for the other wavenumbers being obtained by a simple scaling procedure. The square root velocity profile combined with a k^{-3} wave spectrum can be regarded as having "self-similar" geometry. Finally, in calculating the drag coefficient, the velocity profile is made logarithmic for $z > z_p$ (with a continuous gradient at $z = z_p$), consistent with usual constant-stress turbulent boundary layer theory. The inconsistency between the square root "Rayleigh equation" profile and the logarithmic "drag coefficient" profile is the price to be paid for the inexpensive computation.

2. Mathematical formulation

a. *Self-similar sea surface geometry and velocity profile*

We shall assume that the sea surface displacement $\eta(x, t)$ is given by random superposition of many long-crested deep-water linear gravity waves propagating in the positive x direction:

$$\eta(x, t) = \mathrm{Re} \sum_k \tilde{\eta}_k e^{ik(x-ct)}, \quad k > 0, \tag{8}$$

where the Fourier coefficients $\tilde{\eta}_k$ are independent random variables with complex normal distributions, $c = (g/k)^{1/2}$ is the appropriate phase speed, and "Re" gives the real part of a complex quantity. The spectrum of the sea surface variance (energy spectrum, power spectrum, wavenumber spectrum) $E(k)$ can be defined by its integral over intervals $[k_1, k_2]$:

$$\left\langle \sum_{k\in[k_1,k_2]} |\tilde{\eta}_k|^2 \right\rangle = 2\int_{k_1}^{k_2} E(k)dk, \quad 0 < k_1 < k_2, \tag{9}$$

where $\langle \cdot \rangle$ denotes an ensemble average or the mathematical expectation. The integral of $E(k)$ over all wavenumbers gives the variance of the sea surface displacement,

$$\int_0^\infty E(k)dk = \langle \eta^2 \rangle = \left(\frac{H_{m0}}{4}\right)^2, \tag{10}$$

H_{m0} being the significant wave height.

It is common to assume that the high-wavenumber tail of the ocean surface gravity wave spectrum is of the form

$$E(k) \sim \beta k_p^{-3+p} k^{-p}, \quad k \to \infty, \qquad (11)$$

where p and β are dimensionless parameters, and k_p is the wavenumber at the spectral peak, where $E(k)$ has its maximum value. The sea surface generated with this type of spectrum, when viewed at length scales $L \ll k_p^{-1}$, is *statistically self-affine* (Mandelbrot 1983, chapter 39). Using (11), (9), and (8), we can see that if we multiply the horizontal dimensions by a factor r_x and the vertical dimensions by a factor $r_z = r_x^{(p-1)/2}$, we obtain a new sea surface that looks statistically identical to the old one at such small scales (Glazman 1986; Glazman and Weichman 1989). If $p = 3$, corresponding to Phillips' (1958) equilibrium spectral range, we have $r_z = r_x$ and the sea surface is statistically self-*similar*, so that the small-scale structure appears (statistically) unchanged under a simple magnification or reduction.

That the sea surface form may be (statistically) self-similar for $E(k) \propto k^{-3}$ suggests that other aspects of the wind–wave system may be self-similar as well. Specifically, the wind velocity profile $U(z)$ may have a self-similarity property when observed in conjunction with the sea surface. This will be the case if, for each wavenumber k, the relevant critical height $z_c(k)$ is a constant multiple of the inverse wavenumber k^{-1}, that is, $kz_c(k) = \text{const} = K$. This means that

$$U(z) = c(Kz^{-1}) = \left(\frac{g}{K}\right)^{1/2} z^{1/2}, \qquad (12)$$

that is, the wind velocity has a square root profile. Although this profile is different from the generally accepted logarithmic profile, it shares the property of negative curvature. Since wind–wave resonant interaction will disappear for $z > z_p \equiv z_c(k_p)$, we can expect a transition to a logarithmic profile above $z = z_p$.

For the simplified model presented here, we shall use the simple wave spectrum [cf. Kitaigorodskii 1973, Eq. (2.27); Nordeng 1991]

$$E(k) = \begin{cases} 0, & k < k_p \\ \frac{1}{2}\alpha_p k^{-3}, & k_p \leqslant k < \infty. \end{cases} \qquad (13)$$

The wind velocity is specified by (12) for $z \leqslant z_p = K/k_p$, and by a logarithmic profile for $z \geqslant z_p$, the wind velocity and its gradient dU/dz being continuous at $z = z_p$:

$$U(z) = \begin{cases} (g/K)^{1/2} z^{1/2}, & 0 \leqslant z \leqslant z_p \\ c_p + (U_*/\kappa)\log[(z - z_1)/(z_p - z_1)], & \\ & z_p \leqslant z < \infty, \end{cases} \qquad (14)$$

where $c_p = (g/k_p)^{1/2}$ and

$$z_1 = z_p\left(1 - \frac{2U_*}{\kappa c_p}\right). \qquad (15)$$

Figure 1 shows an example of such a velocity profile.

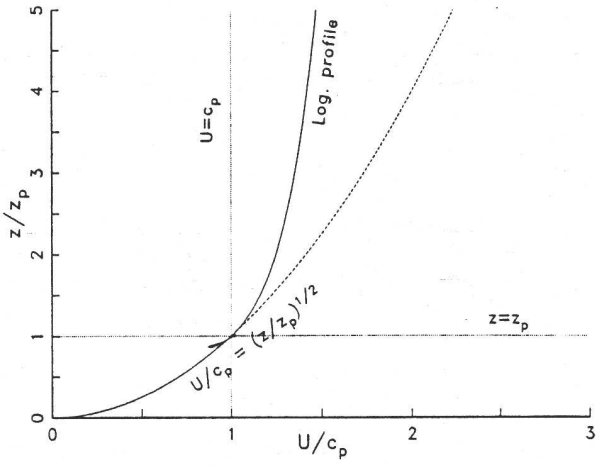

FIG. 1. Example of the wind velocity profile used in the simplified model, for $K = 0.15$ and $c_p/U_* = 12.89$, showing the square root and logarithmic sections.

b. *Wave generation*

According to Miles's (1957) theory of wave generation, the rate at which energy is transferred from the wind to waves of wavenumber k, $\rho_w g \dot{E}_{\text{in}}(k)$, is given by

$$\frac{\dot{E}_{\text{in}}(k)}{E(k)} = \frac{\sigma}{\rho_w g} \operatorname{Im} \frac{\tilde{p}_k(0)}{\tilde{\eta}_k} = -\pi \frac{\rho}{\rho_w} c(k) \left[|\chi_k|^2 \frac{d^2U/dz^2}{|dU/dz|} \right]_{z=z_c(k)}, \qquad (16)$$

ρ_w being the water density, $\tilde{p}_k(0)$ being the Fourier coefficient of the sea surface pressure at wavenumber k, and "Im" denoting the imaginary part. The quantity χ_k is the Fourier coefficient of the vertical velocity component at wavenumber k, normalized so that $\chi_k(0) = 1$ and $\chi_k(\infty) = 0$. It satisfies the Rayleigh equation (3) (cf. Janssen 1982, 1989). For the square root velocity profile in (14), extended above z_p to apply for $0 \leqslant z < \infty$, (3) becomes

$$\frac{d^2\chi}{d\zeta^2} + \left[\frac{\zeta^{-3/2}}{4(\zeta^{1/2} - 1)} - K^2\right]\chi = 0, \qquad (17)$$

where the k subscript has been dropped, $\zeta = z/[z_c(k)]$, and $K = kz_c(k)$. Equation (16) becomes

$$\frac{\rho_w}{\rho} \frac{\dot{E}_{\text{in}}(k)}{\sigma E(k)} = \frac{\pi}{2} |\chi_c|^2 K^{-1}, \qquad (18)$$

where $\chi_c = \chi_k(z_c)$.

Since K is independent of k for a square root velocity profile, we thus need only solve the single ordinary differential equation (17) in order to determine $\dot{E}_{\text{in}}(k)/E(k)$ for all k. This is done using the method of Conte

and Miles (1959), after transforming the independent variable in (17) to $\xi = \zeta^{1/2}$:

$$\frac{d^2\chi}{d\xi^2} - \frac{1}{\xi}\frac{d\chi}{d\xi} + \left[\frac{1}{\xi(\xi-1)} - 4K^2\xi^2\right]\chi = 0. \quad (19)$$

This equation has regular singularities at $\xi = 0$ (the sea surface) and $\xi = 1$ (the critical level). About $\xi = 0$, the solutions to the differential equation can be expressed as power series:

$$\chi = A_{01}\left(\xi^2 + \tfrac{1}{3}\xi^3 + \cdots\right),$$

$$\chi = A_{02}\left[1 - \xi - \frac{15(K^2+7K^4)}{2(45+23K^2)}\xi^2 - \frac{5(K^2+7K^4)}{2(45+23K^2)}\xi^3 + \cdots\right]. \quad (20)$$

About the critical level, one of the solutions, χ_1, can be represented by a power series, but the expansion of the other solution, χ_2, involves a logarithm:

$$\chi_1 = A_{11}\left[(\xi-1) + \tfrac{2}{3}K^2(\xi-1)^3 + \cdots\right], \quad (21)$$

$$\chi_2 = \begin{cases} A_{12}(\chi_1 \log|\xi-1| + \chi_3), & \xi > 1 \\ A_{12}[\chi_1(\log|\xi-1| - i\pi) + \chi_3], & \xi < 1, \end{cases} \quad (22)$$

where $\chi_3 = -1 - 2K^2(\xi-1)^2 - (20/9)K^2(\xi-1)^3 + \cdots$. The term $-i\pi$, which appears in (22) for $\xi < 1$, is a consequence of the fact that the path of integration of (19) must pass below the singularity at $\xi = 1$ (Tollmien 1931; Lin 1955). The symbols A_{01}, A_{02}, A_{11}, and A_{12} are arbitrary constants.

As in Conte and Miles (1959), the power series solution χ_1 and the logarithmic solution χ_2 were both determined by numerical integration from just above $\xi = 1$ to some suitability large value of ξ, using a fourth-order Runge–Kutta technique. An initial value of $\xi = 1 + \epsilon$, $\epsilon = 10^{-4}$, was used, the results being checked for accuracy by repeating the integration for $\epsilon = 10^{-7}$. The initial value of χ_1 and χ_2 were specified to $O(\epsilon)$ and their derivatives to $O(1)$.

The integration steps were made variable, increasing in geometric ratios of approximately 1.1 from an initial size of ϵ until a suitable small constant value was reached. At the upper limit of integration, χ_1 and χ_2 were added together in such proportions that their sum was equal to zero, thus satisfying approximately the boundary condition $\chi(\infty) = 0$. The combined solution was then integrated downwards from $\xi = 1 - \epsilon$ to $\xi = 0 + \epsilon$, using steps that increased geometrically and then decreased geometrically as the lower limit was approached. As before, the initial value was specified to $O(\epsilon)$. After the integration was completed, the result was scaled so that $\chi(0 + \epsilon) = 1$, satisfying approximately the lower boundary condition for χ. For $0.01 \leqslant K \leqslant 10$, the real and imaginary parts of χ_c never varied by more than 1 in the fourth decimal place when ϵ was changed from 10^{-4} to 10^{-7}.

c. *Wave and turbulent stresses*

The downward momentum flux due to wave-associated motions is equal to the wave stress τ_w, which satisfies

$$\frac{d\tau_w}{dz} = \rho D \frac{d^2U}{dz^2}, \quad (23)$$

where the wave diffusion coefficient D is given by

$$D(z) = 2\pi c k^2 |\chi_c|^2 E(k), \quad c(k) = U(z), \quad (24)$$

(Fabrikant 1976; Janssen 1982, 1989). Using (16), some algebraic manipulation shows that the change in τ_w at a critical height $z_c(k)$ is equal to the flux of momentum to the appropriate component of the wave spectrum, $(\rho_w g/c)\dot{E}_{in}(k)$, that is,

$$\frac{d\tau_w}{dz_c(k)} = \frac{\rho_w g \dot{E}_{in}(k)}{c(k)}\left[\frac{dz_c(k)}{dk}\right]^{-1}. \quad (25)$$

If we use the wave spectrum (13) and the wind profile (14), $d\tau_w/dz$ becomes constant and negative for $z < z_p$. Setting $\tau_w(\infty) = 0$, we have

$$\tau_w(z) = \begin{cases} \rho U_*^2[1 - (z/z_p)], & 0 \leqslant z \leqslant z_p \\ 0, & z \geqslant z_p, \end{cases} \quad (26)$$

with

$$U_*^2 = \tfrac{1}{4}\pi\alpha_P K^{-1} c_p^2 |\chi_c|^2. \quad (27)$$

The wave stress τ_w decreases linearly from ρU_*^2 to zero as we move from the sea surface up to z_p. This contrasts with the model of Chalikov and Makin (1991) in which τ_w has step function behavior, being a constant fraction of ρU_*^2 at and near the surface (in the runs they presented, the fraction lies between about 0.2 and 0.8), and decreasing in a single step to zero at an empirically determined level (at $z \propto k_p^{-3.32}$).

Note that if we combine (27) with (18) we obtain a relation between the rate of wave generation and U_* that does not involve χ_c:

$$\frac{\rho_w}{\rho}\frac{\dot{E}_{in}(k)}{\sigma E(k)} = 2\alpha_P^{-1}\left(\frac{U_*}{c_p}\right)^2. \quad (28)$$

So the wave generation rate is determined by the wave age c_p/U_* and the Phillips parameter α_P. In fact this is not surprising, since we assume that all the air–sea momentum flux is taken up by the waves, and distributed to the different wavenumber components in fixed ratios.

If we neglect molecular viscosity, the difference between the total applied stress ρU_*^2 and τ_w must be accounted for by the turbulent shear stress τ_t, so

$$\tau_t(z) = \begin{cases} \rho U_*^2(z/z_p), & 0 \leqslant z \leqslant z_p \\ \rho U_*^2, & z \geqslant z_p. \end{cases} \quad (29)$$

We can relate (29) to the Prandtl (1925) mixing length formulation for the turbulent shear stress ($\tau_t = \rho l^2 |dU/dz| dU/dz$), and to the eddy viscosity formulation ($\tau_t = \rho \nu_T dU/dz$), if the mixing length l is given by

$$l = \begin{cases} 2(U_*/c_p)z, & 0 \leqslant z \leqslant z_p \\ \kappa(z - z_1), & z \geqslant z_p, \end{cases} \quad (30)$$

and the eddy viscosity ν_T is given by

$$\nu_T = \begin{cases} 2(U_*^2/c_p)(z^{3/2}/z_p^{1/2}), & 0 \leqslant z \leqslant z_p \\ \kappa U_*(z - z_1), & z \geqslant z_p. \end{cases} \quad (31)$$

Using the definition (15) of z_1, it can be seen that both l and ν_T are continuous at $z = z_p$. Examples of the profiles of l and ν_T are shown in Figs. 2 and 3. We can justify the change in the slope of the mixing length profile for $z < z_p$ by the fact that wave-associated motions carry some of the shear stress that would otherwise have been carried by the turbulence. We can write ν_T as the product of the mixing length l and a velocity scale v, where

$$v = \begin{cases} U_*(z/z_p)^{1/2}, & 0 \leqslant z \leqslant z_p \\ U_*, & z \geqslant z_p. \end{cases} \quad (32)$$

In fact, we can write $\nu_T = l(\tau_t/\rho)^{1/2}$ for all z, so the velocity scale v is a modified friction velocity.

d. Other spectra and velocity profiles

If we let the power law p of the wave energy spectrum in (11) be different from 3, then the small-scale structure of the sea surface can no longer be self-similar, only self-affine, with $r_z \neq r_x$. If we apply the same geometrical argument as we applied for the self-similar case, the ratio of critical height to inverse wavenumber, kz_c, should be proportional to $(r_z^{-1})/(r_x^{-1})$, since z_c is a vertical dimension and k^{-1} is a horizontal one. Since $r_x \propto k$, we have

$$kz_c(k) = K_p k^{(3-p)/2}, \quad (33)$$

where K_p is a constant, and the velocity profile becomes

$$U(z) = g^{1/2}(z/K_p)^{1/(p-1)}. \quad (34)$$

The energy flux to the waves is then given by

$$\frac{\rho_w}{\rho}\frac{\dot{E}_{in}(k)}{\sigma E(k)} = \pi \frac{p-2}{p-1} |\chi_c|^2 K_p^{-1} k^{(p-3)/2}, \quad (35)$$

so that $\dot{E}_{in}(k)/[\sigma E(k)]$ is no longer independent of k. For example, if $p < 3$, as in the theory of Phillips (1985), which predicts $p = 5/2$, $k^{(p-3)/2}$ obviously decreases with k and $|\chi_c|^2$ also decreases with k, in fact very rapidly at large wavenumbers where $kz_c \gg 1$. The momentum flux to the various wavenumber components will be given by

$$\dot{\Pi}_{in}(k) \propto |\chi_c|^2 k^{-(p+1)/2}. \quad (36)$$

For $p < 3$, the $k^{-(p+1)/2}$ factor will tend to push the support of the momentum flux to higher wavenumbers than for $p = 3$, but the $|\chi_c|^2$ factor will have the opposite effect. The end result is difficult to predict without performing an explicit computation of χ_c for a whole range of kz_c with a velocity profile of the form (34). I would, however, expect the resulting behavior of the overall drag coefficient to be rather similar to the predictions in the next section, provided that p is not too different from 3.

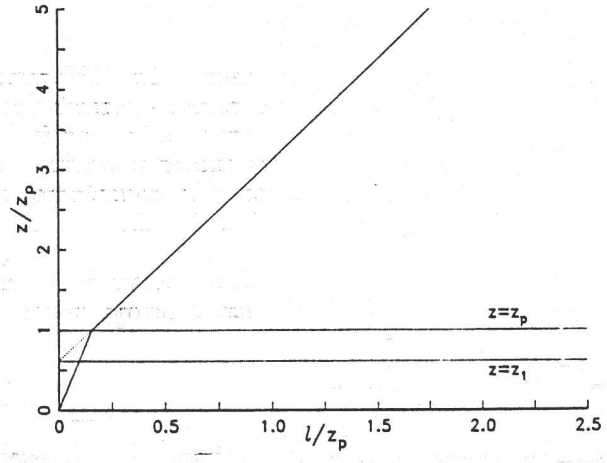

FIG. 2. Example of the profile of mixing length l, for $c_p/U_* = 12.89$.

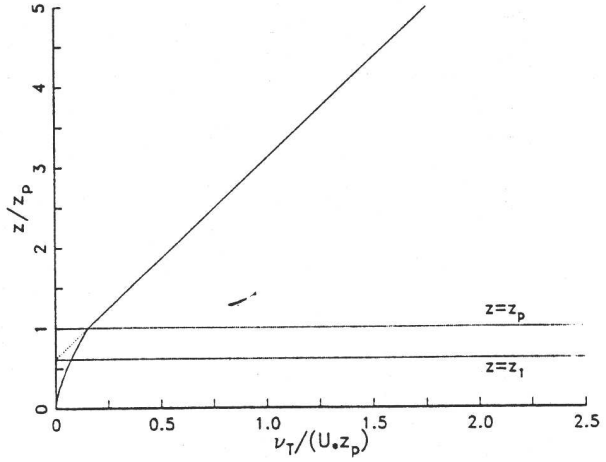

FIG. 3. Example of the profile of eddy viscosity ν_T, for $c_p/U_* = 12.89$.

3. Results

An example of the vertical profile of χ is shown in Fig. 4. The effect of the singularity at $z = z_c$ is a kink in the real part of χ and an infinite derivative for the

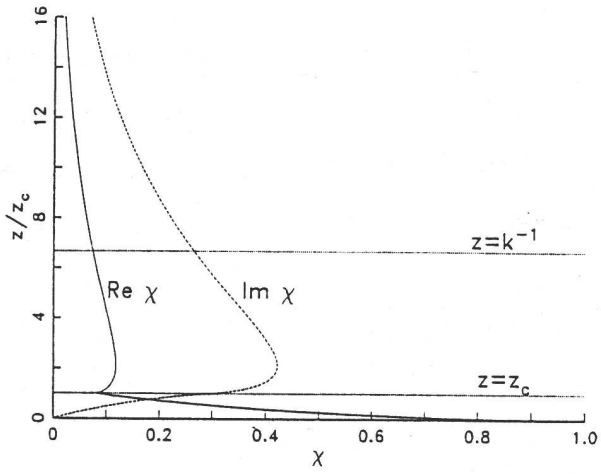

FIG. 4. Example of the solution of the Rayleigh equation for a square root velocity profile, $K = 0.15$.

imaginary part. Table 1 shows the value of χ_c as a function of K, together with the nondimensional wave generation factor, $(\rho_w/\rho)\sigma^{-1}\dot{E}_{in}(k)/E(k) = (\pi/2)|\chi_c|^2K^{-1}$. From (28) we can relate wave generation to the wave age if we know the Phillips parameter α_P, for which a variety of formulations are reported in the literature. In this paper, results using three different formulations will be compared. The first is the constant value,

$$\alpha_P = 0.0081, \tag{37}$$

reported by Pierson and Moskowitz (1964). In the other two formulations, α_P depends on the wave age, c_p/U_*:

$$\alpha_P = 0.054(c_p/U_*)^{-2/3}, \tag{38}$$

$$\alpha_P = 0.57(c_p/U_*)^{-3/2}. \tag{39}$$

TABLE 1. Solution of Rayleigh equation at the critical level (χ_c) and nondimensional wave generation factor $(\rho_w/\rho)\sigma^{-1}\dot{E}_{in}(k)/E(k) = (\pi/2)|\chi_c|^2K^{-1}$ for various values of $K \equiv kz_c$.

K	$\mathrm{Re}\chi_c$	$\mathrm{Im}\chi_c$	$\frac{\pi}{2}\lvert\chi_c\rvert^2K^{-1}$
0.010	−0.1041	+0.2795	13.97
0.015	−0.0859	+0.2931	9.768
0.02	−0.0708	+0.3017	7.543
0.03	−0.0462	+0.3114	5.193
0.05	−0.0097	+0.3179	3.178
0.07	+0.0173	+0.3172	2.265
0.10	+0.0476	+0.3106	1.551
0.15	+0.0824	+0.2942	0.9775
0.2	+0.1057	+0.2760	0.6860
0.3	+0.1333	+0.2405	0.3959
0.5	+0.1513	+0.1809	0.1747
0.7	+0.1483	+0.1363	0.0910
1.0	+0.1300	+0.0899	0.0392

Equations (38) and (39) were employed by Janssen (1989), using different interpretations of the JONSWAP results (Hasselmann et al. 1973). The three equations (37)–(39), or at least their power laws, appear to encompass all reasonable observations of wind seas under neutrally stratified conditions. To take a more recent example, stereophotographic observations of short gravity waves performed by Banner et al. (1989) give results close to (37): the power law that they found, $\alpha_P \propto (c_p/U_*)^{(-0.18\pm0.18)}$, gives a rather slow variation of α_P, and their constant of proportionality is not too different from that in (37).

Using the three different relations, we obtain:

$$\frac{\dot{E}_{in}(k)}{\sigma E(k)} \approx \begin{cases} 0.31(U_*/c_p)^2, & \alpha_P = 0.0081 \\ 0.046(U_*/c_p)^{4/3}, & \alpha_P = 0.054(c_p/U_*)^{-2/3} \\ 0.0044(U_*/c_p)^{1/2}, & \alpha_P = 0.57(c_p/U_*)^{-3/2}, \end{cases} \tag{40}$$

where we have assumed that $\rho_w/\rho \approx 800$. Graphs of these nondimensional wave generation factors are shown in Fig. 5. For constant α_P, (40) is reminiscent of Plant's (1982) relation,

$$\frac{\dot{E}_{in}(k)}{\sigma E(k)} \approx 0.04\left[\frac{U_*}{c(k)}\right]^2 \cos\theta, \tag{41}$$

also plotted in Fig. 5, but the constant factor is much larger. This can perhaps be justified by noting that for a given wave spectrum, $\sigma^{-1}\dot{E}_{in}(k)/E(k)$ will be linearly proportional to the wavenumber in Plant's formula-

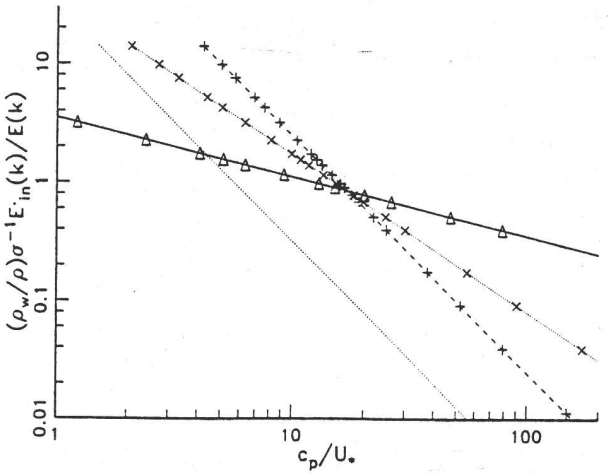

FIG. 5. Nondimensional wave generation factor, $(\rho_w/\rho)\sigma^{-1}\dot{E}_{in}(k)/E(k)$, as a function of wave age c_p/U_*. Open dashed line with plus signs: $\alpha_P = 0.0081$; dotted line with crosses: $\alpha_P = 0.054(c_p/U_*)^{-2/3}$; solid line with triangles: $\alpha_P = 0.57(c_p/U_*)^{-3/2}$; and dotted line without symbols: Plant's (1982) relation (37) with abscissa $c(k)/(U_* \cos^{1/2}\theta)$ instead of c_p/U_*.

tion, whereas it is forced to be constant in the present simplified model. For $\theta = 0$ the two relations are equal at $k/k_p \approx 7.7$ or $\sigma/\sigma_p \approx 2.8$. The other two formulations for α_P give rates of wave generation that are more slowly varying functions of U_*/c_p. If $\alpha_P \propto (c_p/U_*)^{-1}$, we would have a linear relation $\sigma^{-1}\dot{E}_{in}(k)/E(k) \propto (U_*/c_p)$, resembling the formulation $\sigma^{-1}\dot{E}_{in}(k)/E(k) \propto [28U_*/c(k)]\cos\theta - 1$ used in the spectral wave model of Hasselmann et al. (1985), which is in turn based on the field results, $\sigma^{-1}\dot{E}_{in}(k)/E(k) \propto [U(5\text{ m})/c]\cos\theta - 1$, of Snyder et al. (1981).

A comparison with results from the numerical models of Janssen (1989, 1991) and Jenkins (1992) is shown in Fig. 6 for young sea states, with $c_p/U_* = 5$ and $U_* = 0.7$ m s^{-1} for all models except Janssen (1991). The results of Janssen (1991, Fig. 1) are plotted for a logarithmic wind velocity profile with a roughness length that includes the wave effects, given by $\alpha_C = gz_0/U_*^2 = 0.144$, that is, enhanced by a factor of 10. For fully developed sea states, corresponding results are shown in Fig. 7, with $\alpha_C = 0.0144$, that is, without an enhanced roughness length, for Janssen (1991, Fig. 1), and with $c_p/U_* = 25$ and $U_* = 0.7$ m s^{-1} for the other models.

The present model [using Eq. (28)] gives a constant value of $\sigma^{-1}\dot{E}_{in}(k)/E(k)$, defined only for $k \geq k_p$. It is generally greater than the predictions of the other models for the fully developed sea state except in the high-wavenumber tail. For the young sea state it also diverges quite a lot from the other models, but the other models are also in poor agreement with each other for $k > k_p$. The disagreements are not surprising since the simplified model does not permit $\sigma^{-1}\dot{E}_{in}(k)/E(k)$ to vary with wavenumber, as has been discussed above. The momentum flux, computed from (36) with $p = 3$, is predicted to be proportional to k^{-2} by the present model. Hence, it is supported by the whole of the spectrum—alternative (ii) described in section 1b. The momentum flux is somewhat biased to the short wavelengths, compared with the energy flux proportional to $k^{-5/2}$.

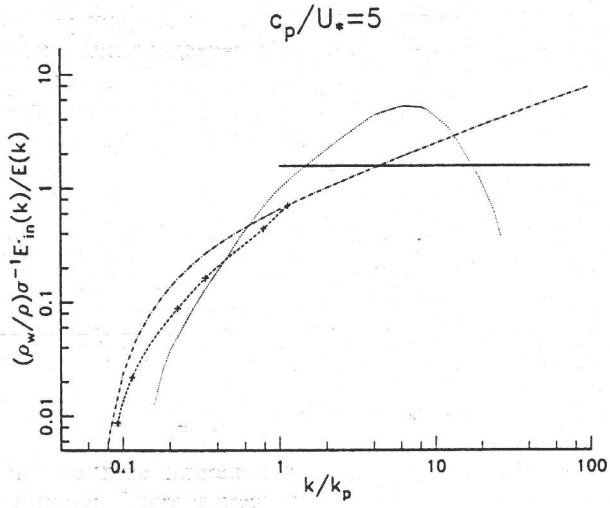

FIG. 6. Nondimensional wave generation factor, $(\rho_w/\rho)\sigma^{-1}\dot{E}_{in}(k)/E(k)$, as a function of wavenumber, for "young" sea state, $c_p/U_* = 5$, with Phillips parameter $\alpha_P = 0.57(c_p/U_*)^{-3/2}$, and friction velocity $U_* = 0.7$ m s^{-1}. Broken line with plus signs: model results of Janssen (1989); dash-dotted line: model results of Jenkins (1992); solid line: present model; dotted line: results from the simple surface-layer model of Janssen (1991) with $\alpha_C = 0.144$.

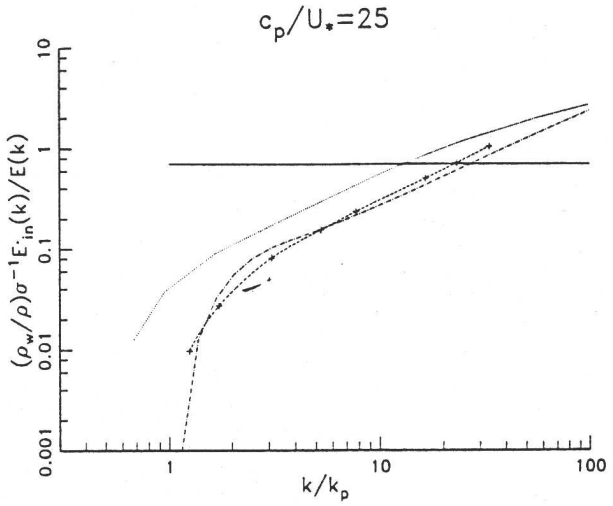

FIG. 7. Nondimensional wave generation factor as a function of wavenumber, for "developed" sea state ($c_p/U_* = 25$), with Phillips parameter $\alpha_P = 0.57(c_p/U_*)^{-3/2}$ and $U_* = 0.7$ m s^{-1}. Broken line with plus signs: model results of Janssen (1989); dash-dotted line: model results of Jenkins (1992); solid line: present model; dotted line: results from the simple surface layer model of Janssen (1991) with $\alpha_C = 0.0144$.

If the spectral exponent p is less than 3, the horizontal straight lines in Figs. 6–7 will be replaced by curved lines of negative slope, the slopes getting steeper with increasing values of k. If $p > 3$ the horizontal lines will be replaced by lines with positive slope.

Figure 8 shows graphs of the modeled drag coefficient referred to a height $z = k_p^{-1}$,

$$C_D(k_p^{-1}) = \left[\frac{U_*}{U(k_p^{-1})}\right]^2 = \left[\frac{c_p}{U_*} + \frac{1}{\kappa}\log\left(\frac{\kappa}{2K}\frac{c_p}{U_*} - \frac{\kappa}{2}\frac{c_p}{U_*} + 1\right)\right]^{-2}, \quad (k_p^{-1} > z_p), \quad (42)$$

as a function of wave age, for the three different formulations of the Phillips parameter. There is greatest difference between the formulations for small c_p/U_*, the difference being small for $c_p/U_* > 15$. The reason for the small differences for larger c_p/U_* is probably because $\log[(c_p/U_*)/K]$ is then a slowly varying function of c_p/U_*, being the same for all three formulations near $c_p/U_* = 17$. [See Fig. 9. The three terms inside

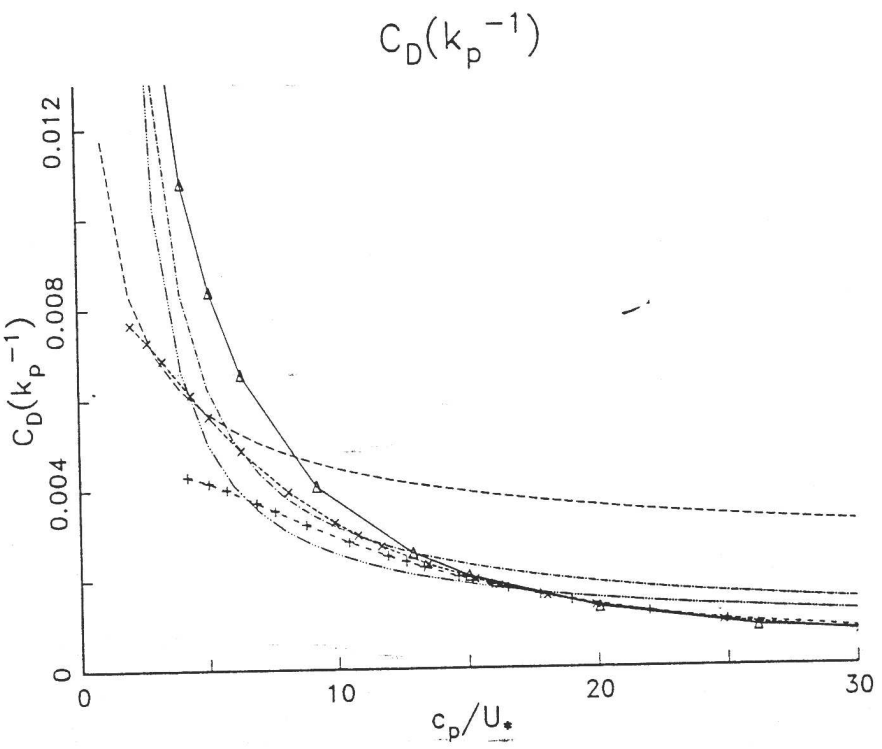

FIG. 8. Drag coefficient at $z = k_p^{-1}$ as a function of c_p/U_*. Lines with symbols: present model; open dashed line with plus signs: $\alpha_P = 0.0081$; close dashed line with crosses: $\alpha_P = 0.054(c_p/U_*)^{-2/3}$; solid line with triangles: $\alpha_P = 0.57(c_p/U_*)^{-3/2}$; lines without symbols: from experimental data; dashed line: from the relation of Toba and colleagues [Toba and Koga 1986, Eqs. (9) and (10)]; dash-dotted line: from HEXMAX measurements in the southern North Sea (Maat et al. 1991); dash-and-three-dots line: from Lake Ontario measurements (Donelan 1990), assuming $\alpha_P = 0.57(c_p/U_*)^{-3/2}$.

the logarithm in (42) are written in decreasing order of absolute value, if $c_p/U_* > 2/\kappa \approx 5$ and $K < 1$.]

In Fig. 8 I also show the drag coefficient obtained from formulas fitted to experimental measurements:

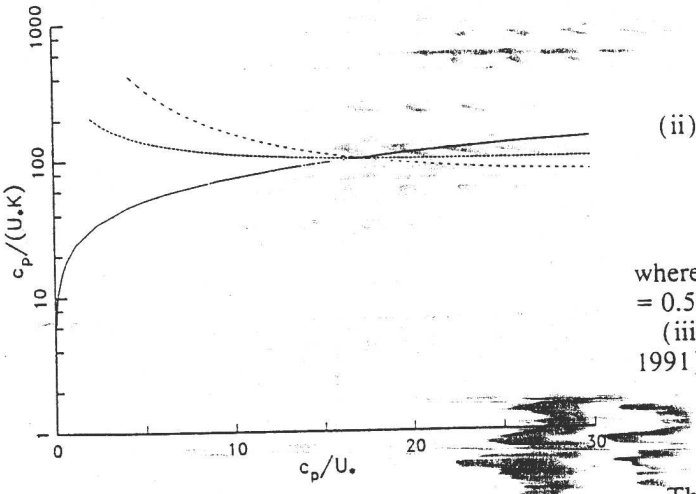

FIG. 9. Semilogarithmic plot of $(c_p/U_*)/K$ against c_p/U_*. Open dashed line: $\alpha_P = 0.0081$; close dashed line: $\alpha_P = 0.054(c_p/U_*)^{-2/3}$; solid line: $\alpha_P = 0.57(c_p/U_*)^{-3/2}$.

(i) from field and laboratory data by Toba and colleagues [Toba 1979; Toba and Koga 1986, Eqs. (9)–(10); Toba et al. 1990, Eq. (3)],

$$C_D(z) = \kappa^2\left[\log\left(\frac{gz}{0.025\,c_p U_*}\right)\right]^{-2}$$

$$\Rightarrow C_D(k_p^{-1}) = \kappa^2\left[\log\left(\frac{c_p}{0.025 U_*}\right)\right]^{-2}; \quad (43)$$

(ii) from Lake Ontario field data (Donelan 1990),

$$\frac{z_0}{\langle\eta^2\rangle^{1/2}} = 1.84\left(\frac{U_*}{c_p}\right)^{2.53}, \quad (44)$$

where I calculate $\langle\eta^2\rangle$ from (10) and (13) with $\alpha_P = 0.57(c_p/U_*)^{-3/2}$; and

(iii) from North Sea HEXMAX data (Maat et al. 1991),

$$\frac{gz_0}{U_*^2} = 0.8\left(\frac{c_p}{U_*}\right)^{-1}. \quad (45)$$

The corresponding nondimensional roughness lengths $k_p z_0$ are shown in Figs. 10 (semilogarithmic plot) and 11 (log–log plot).

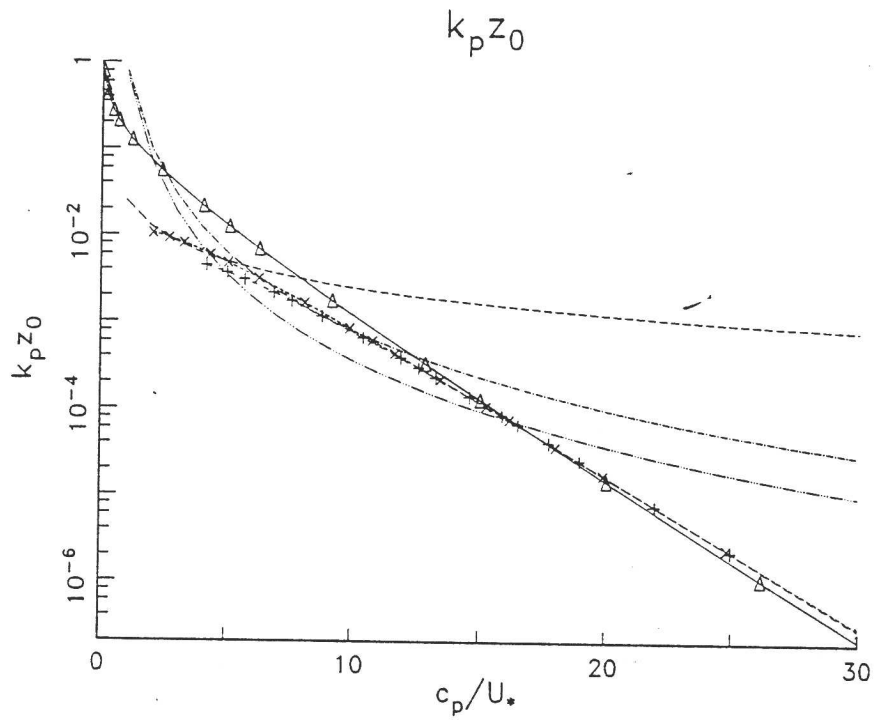

FIG. 10. Semilogarithmic plot of nondimensional roughness length k_pz_0 as a function of wave age c_p/U_*. Line types and symbols as in Fig. 8.

For fully developed seas ($c_p/U_* > 20$) the present model gives significantly lower values for drag coefficient and roughness length than the field observations. The model predicts that the roughness length decreases exponentially with wave age, whereas the field measurements indicate a power-law behavior. For young

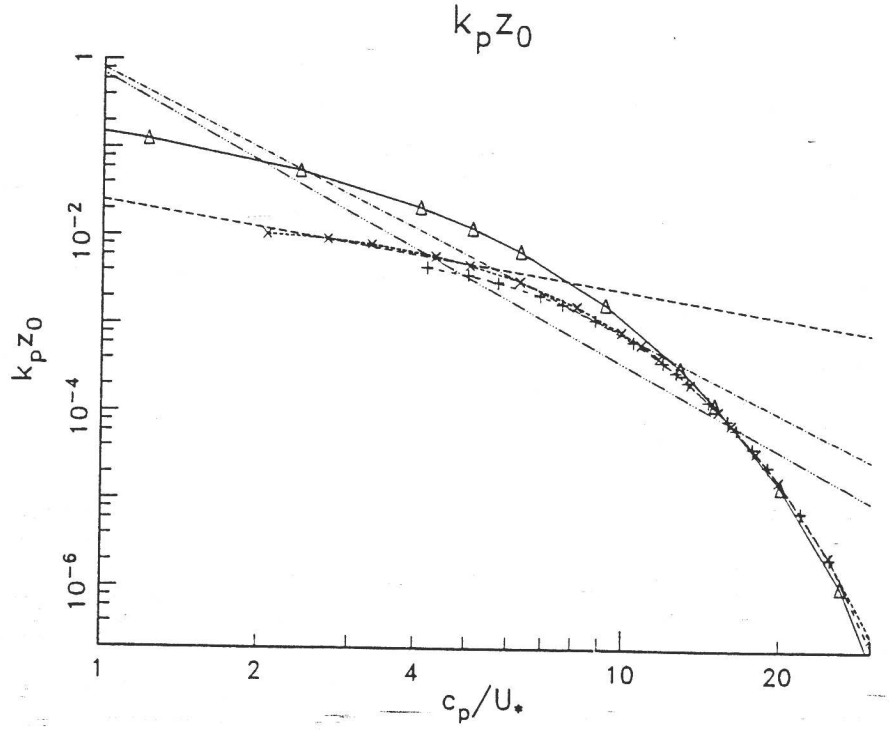

FIG. 11. As in Fig. 10 but plotted on a log–log scale.

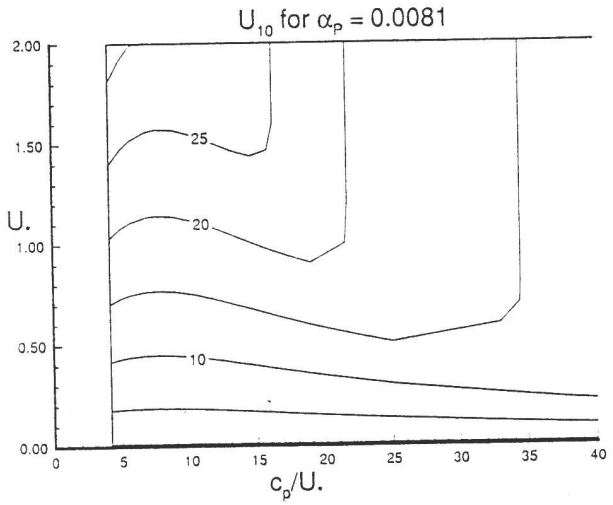

FIG. 12. Contour plot of the wind speed at $z = 10$ m as a function of c_p/U_* and U_*, for constant $\alpha_P = 0.0081$.

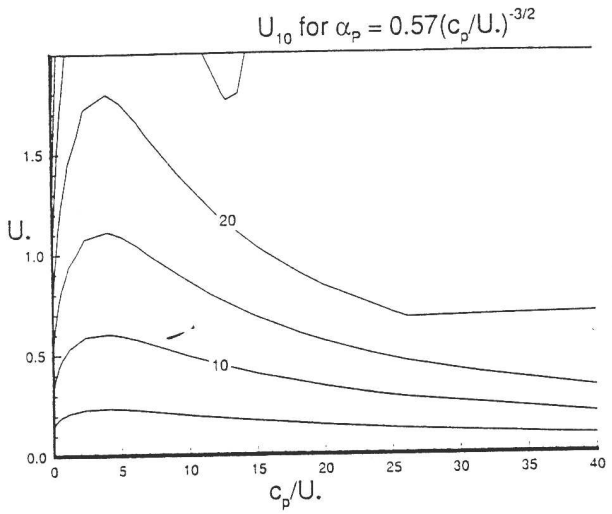

FIG. 14. Contour plot of the wind speed at $z = 10$ m as a function of c_p/U_* and U_*, for $\alpha_P = 0.57(c_p/U_*)^{-3/2}$.

wind seas, the experimental drag coefficient graph of Maat et al. (1991) lies between the model curves for $\alpha_P \propto (c_p/U_*)^{-2/3}$ and $\alpha_P \propto (c_p/U_*)^{-3/2}$; the Donelan (1990) drag coefficients for $\alpha_P \propto (c_p/U_*)^{-3/2}$ are considerably lower than the corresponding predictions of the model.

Results referred to a fixed height of 10 m are shown in Figs. 12–18. Figures 12–14 are contour plots of the wind speed at the 10-m level, as a function of wave age and friction velocity. It can be seen that U_* and $C_D(10\text{ m})$ depend on both wind speed and wave age. If we follow individual wind speed contours along, we can see that the friction velocity first increases with wave age, and then decreases, while the 10-m level is within the "logarithmic" part of the wind profile. The vertically directed contours in the top right-hand parts of the figures correspond to $z_p > 10$ m, so that the 10-m level is in the square root part of the wind profile. From (12) and (27), the constant of proportionality $(g/K)^{1/2}$ is a function of c_p/U_*, $|\chi_c|^2$ and α_P, and since $|\chi_c|^2$ depends just on K and we assume that α_P depends only on c_p/U_*, the wind speed at a specific height must be fixed if c_p/U_* is fixed, independent of U_*. This counterintuitive result will be modified if we let turbulence play a greater role in the region $z < z_p$ and let capillary waves or other roughness elements support some of the momentum flux. It should be pointed out that very few accurate field measurements of wind profiles have been made beneath the critical level z_p over wind seas, particularly if we require $z_p \geq 10$ m. For example, choose $c_p/U_* = 25$ and $U_* = 1.0$ m s^{-1} in Fig. 13. The corresponding sea state has a peak period of 16 sec and a significant wave height of 10.1 m. These are rather severe conditions, and it is unlikely that many wind profile and wind stress measurements are available under such circumstances with instruments situated so close to the sea surface.

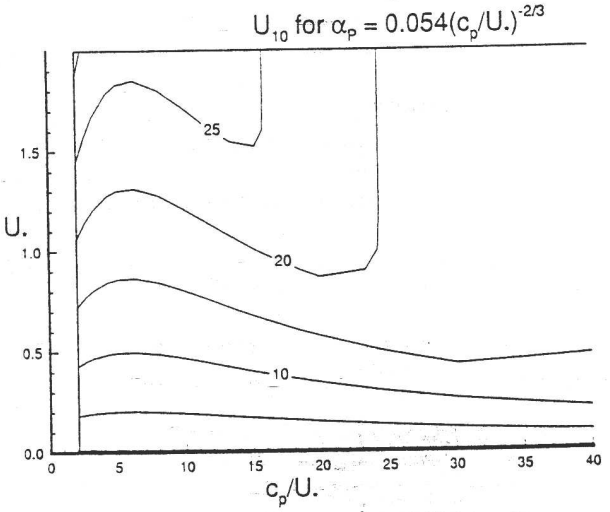

FIG. 13. Contour plot of the wind speed at $z = 10$ m as a function of c_p/U_* and U_*, for $\alpha_P = 0.054(c_p/U_*)^{-2/3}$.

Figures 15–18, which show the drag coefficient referred to the 10-m level, correspond to taking horizontal slices through the preceding figures at $U_* = 0.7$ m s^{-1} and $U_* = 0.3$ m s^{-1}, using the three formulas for α_P. Experimental results are shown, using the formulas (43)–(45), but note that $\alpha_P = 0.054(c_p/U_*)^{-2/3}$ is used to calculate $\langle \eta^2 \rangle$ for the Donelan (1990) curve in Fig. 18. In addition, I show the parameterization of North Sea measurements by Geernaert et al. (1987), which is supposed to hold for a large range of U_* values:

$$C_D(10\text{ m}) = 0.012\left(\frac{c_p}{U_*}\right)^{-2/3}. \qquad (46)$$

Model results of Janssen (1989) and Jenkins (1992)

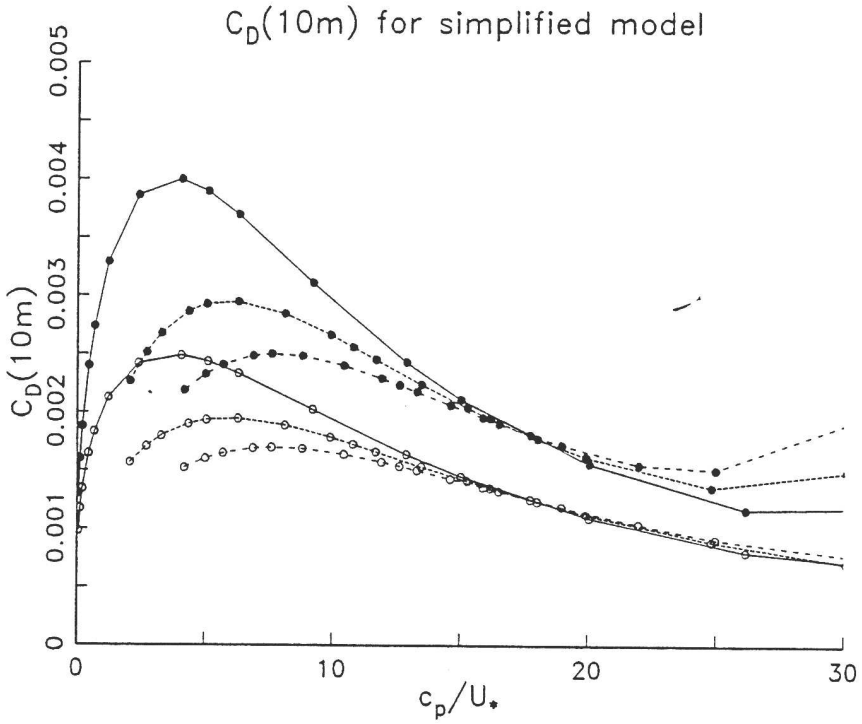

FIG. 15. Drag coefficient for $z = 10$ m from the present model. Open dashed lines: $\alpha_P = 0.0081$. With open circles, $U_* = 0.3$ m s^{-1}; with solid circles, $U_* = 0.7$ m s^{-1}; close dashed lines (short dashes): $\alpha_P = 0.054(c_p/U_*)^{-2/3}$. With open circles, $U_* = 0.3$ m s^{-1}; with solid circles, $U_* = 0.7$ m s^{-1}; solid lines: $\alpha_P = 0.57(c_p/U_*)^{-3/2}$. With open circles, $U_* = 0.3$ m s^{-1}; with solid circles, $U_* = 0.7$ m s^{-1}.

are also presented, and, in Fig. 16, an example of Nordeng's (1991, Fig. 4a) model results for $U_* = 0.7$ m s^{-1}. The model of Janssen (1991) can be expected to follow quite closely the drag coefficient results of Janssen (1989), since the latter model was used as a basis for developing the former. The model of Chalikov and Makin (1991) also has similar behavior to that of Janssen (1989). For Fig. 16, for example, Chalikov and Makin (1991) predict $C_D(10\text{ m}) \approx 1.5 \times 10^{-3}$ for $c_p/U_* = 33$, increasing to 3×10^{-3} for $c_p/U_* = 3.5$, if we use their Fig. 4e with surface roughness scale $\lambda_r = 7 \times 10^{-3}$. For $\alpha_P \propto (c_p/U_*)^{-2/3}$, Chalikov and Makin (1991) also predict only a slow variation of C_D with wave age.

For the present, simplified model, if we hold U_* constant, $C_D(10\text{ m})$ increases to a maximum value as the wave age increases, and then decreases. This behavior occurs for all three parameterizations of α_P. The tendency for $C_D(10\text{ m})$ to increase again for old wind seas corresponds to the 10-m level "moving" from the logarithmic part of the wind velocity profile to the square root part. The drag coefficient's increase with wave age for young seas is in general agreement with the formula of Toba and colleagues (Toba and Koga 1986), but that formula is certainly inconsistent with the other experimental results, which show a decrease of $C_D(10\text{ m})$ with increasing wave age. The Nordeng (1991) model shows the same type of drag coefficient behavior as the present model, but its drag coefficient maximum occurs at a significantly greater wave age.

After the maximum, the simplified model's drag coefficient decreases more rapidly with c_p/U_*, in Figs. 16–18, than the other models and experimental data analyses [except for the Geernaert et al. (1987) results, which may be subject to a systematic decrease of U_* with increasing wave age]. This indicates that the present model with $\alpha_P \propto (c_p/U_*)^{-3/2}$ or $\alpha_P \propto (c_p/U_*)^{-2/3}$ underestimates the effective surface roughness for old sea states. The more computationally expensive models of Janssen (1989) and Jenkins (1992) with $\alpha_P \propto (c_p/U_*)^{-3/2}$ show better agreement with the experimental observations, as do the simple models of Janssen (1991) and Chalikov and Makin (1991). It is possible that we may be modeling a manifestation of "ultrasmoothness" of the sea surface, a topic discussed by Donelan (1990). Note that the simplified model neglects the effect of mean skin friction: it assumes that the molecular viscosity ν is vanishingly small. Thus, there is nothing to prevent the model results from giving a value of z_0 less than that predicted for the flow of air (with its true molecular viscosity) over an aerodynamically smooth surface (Schlichting 1968).

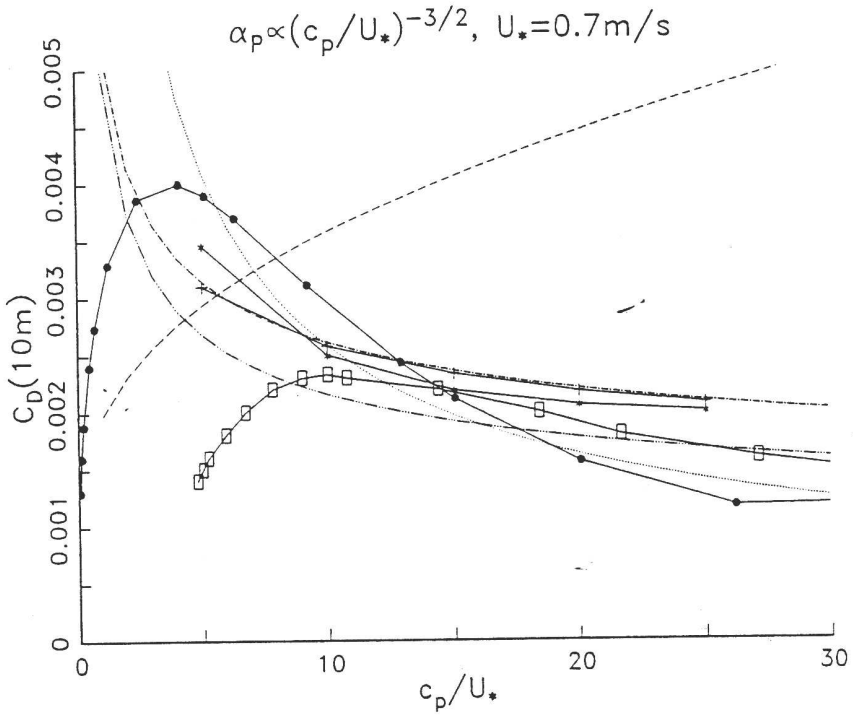

FIG. 16. Drag coefficient for z = 10 m with Phillips parameter $\alpha_P = 0.57(c_p/U_*)^{-3/2}$ and friction velocity U_* = 0.7 m s^{-1}. Solid lines: Model results. With solid circles, present model: with asterisks, Janssen (1989); with plus signs, Jenkins (1992); with rectangles, Nordeng (1991); dotted line: curve fitted by Geernaert et al. (1987) to field experimental results with a range of values of U_*; close dashed line (long dashes): from the relation of Toba and colleagues [Toba and Koga 1986, Eqs. (9) and (10)]; dash-dotted line: from HEXMAX measurements (Maat et al. 1991); dash-and-three-dots line: from Lake Ontario measurements (Donelan 1990).

4. Conclusions

The simplified model for wave generation and air–sea momentum flux presented in this paper is based, as are the numerical models of Janssen (1989) and Jenkins (1992), on a quasi-linear approximation to the hydrodynamic equations. Denoting the characteristic wave amplitude by a, mean quantities of order a^2, such as wave momentum, are taken into account, but fluctuating quantities are only considered to $O(a)$. In common with Janssen's (1989) model, viscosity and turbulence are neglected when considering the behavior of the wave-induced velocity fluctuations in the atmospheric boundary layer, so that Miles' (1957) wave generation theory can be applied, and the resulting Rayleigh equation is solved by the method of Conte and Miles (1959). The iterative procedure used in the Janssen (1989) model and its rather expensive computation of the wind velocity profile on a fine mesh are avoided by prescribing the form of the profile in advance, using a combination of a logarithmic profile above the highest critical level z_p and a square root profile below that height.

The simplified model avoids the explicit specification of a surface roughness parameter. Instead, it assumes that the ocean surface gravity waves provide the effective roughness: as energy is transferred to the waves, there is a corresponding momentum flux, and 100 percent of the available momentum is assumed to be taken up by the waves. The very simple form (13) is used for the wave energy spectrum, and for each wavenumber k, the critical height at which the phase speed $c(k) = (g/k)^{1/2}$ is equal to the wind speed is assumed to be a constant fraction of k^{-1}. This assumption is based on the self-similarity property of the k^{-3} tail of the wave spectrum, and leads to the square root velocity profile mentioned above. Assuming that the downward momentum flux is the sum of a turbulent shear stress τ_t and a wave stress τ_w, we then find that τ_t increases linearly from zero at $z = 0$ to ρU_*^2 at $z = z_p$, with τ_w having a corresponding linear decrease. The effective mixing length, eddy viscosity, and velocity scale, which can be considered to contribute to τ_t, have plausible vertical profiles [see Figs. 2–3 and Eqs. (3)–(32)].

Wave generation rates predicted by the simplified model, together with those predicted by the models of Janssen (1989, 1991) and Jenkins (1992), are shown in Figs. 5–7. When discussing the factors that affect the generation rates, it is important to distinguish between (i) the variation of the generation rate between

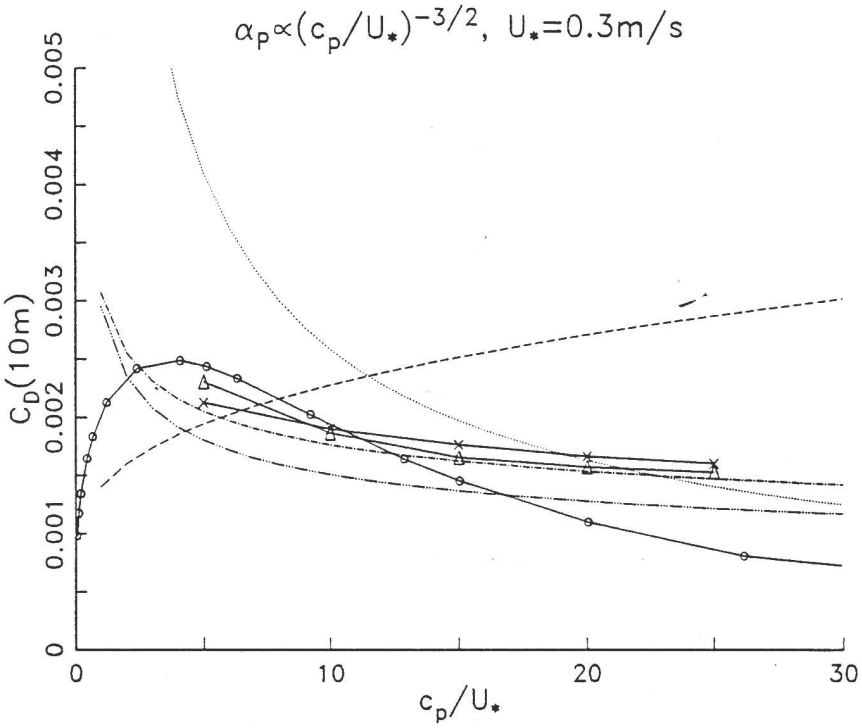

FIG. 17. Drag coefficient for $z = 10$ m with $\alpha_P = 0.57(c_p/U_*)^{-3/2}$ and $U_* = 0.3$ m s^{-1}. Solid lines: model results—with open circles, present model; with triangles, Janssen (1989); with crosses, Jenkins (1992). Dotted line: curve fitted by Geernaert et al. (1987) to field experimental results with a range of values of U_*. Close dashed line (long dashes): from the relation of Toba and colleagues [Toba and Koga 1986, Eqs. (9) and (10)]. Dash-dotted line: from HEXMAX measurements (Maat et al. 1991). Dash-and-three-dots line: from Lake Ontario measurements (Donelan 1990).

different wave spectra and (ii) the distribution of the generation rate within a wave spectrum. The assumptions behind the simplified model restrict $\sigma^{-1}\dot{E}_{in}(k)/E(k)$ to be independent of wavenumber within any one wave spectrum. They do allow $\sigma^{-1}\dot{E}_{in}(k)/E(k)$ to vary between different spectra, and it is predicted to depend only on the Phillips parameter α_P, the wave age c_p/U_* and the density ratio ρ/ρ_w. If α_P is constant, we have $\sigma^{-1}\dot{E}_{in}(k)/E(k) \propto (c_p/U_*)^{-2}$; if $\alpha_P \propto (c_p/U_*)^{-3/2}$ then $\sigma^{-1}\dot{E}_{in}(k)/E(k) \propto (c_p/U_*)^{-1/2}$. It should be noted that there is not much information available from field experiments to determine the spectral distribution of the rate of wave generation (Donelan 1990), particularly in the high-frequency tail.

It may be possible to improve wave generation rate predictions by using spectral tail formulations that are different from k^{-3}, which would then be self-affine rather than self-similar, together with velocity profiles with a power law different from 1/2 (or, indeed, a logarithmic profile). If we were to increase the computational effort, we could use the actual velocity profile in the Rayleigh equation, rather than the artificially extrapolated square root profile employed here.

The drag coefficients predicted by the simplified model, although differing in a number of respects from experimental results, do behave in a reasonable manner under the circumstances. Figures 12–14 indicate that U_*, and thus the drag coefficient, depends on both wind speed and wave age. The nondimensional roughness length $k_p z_0$ decreases exponentially with wave age for old wind seas (if we hold U_* constant), rather than according to the power laws suggested by the fits to field observations of Donelan (1990) and Maat et al. (1991), and the drag coefficients in consequence become significantly lower than these curve fits indicate. This may be a manifestation of a tendency towards "ultrasmoothness," discussed by Donelan (1990). The assumptions employed in formulating the simplified model mean that at the sea surface we should have aerodynamically smooth flow for a fluid with viscosity $\nu \to 0$, since $\tau_t \to 0$ as $z \to 0$.

If we refer the drag coefficient to a fixed level (10 m) and consider fixed values of wind stress or friction velocity, we find that C_D increases with wave age for very young wind seas if U_* is held constant. This is physically reasonable, since very young seas have very small wave heights, and thus can be expected to have low roughness. The formula fitted by Toba and colleagues [Toba and Koga 1986, Eqs. (9)–(10)] makes the drag coefficient increase monotonically with wave

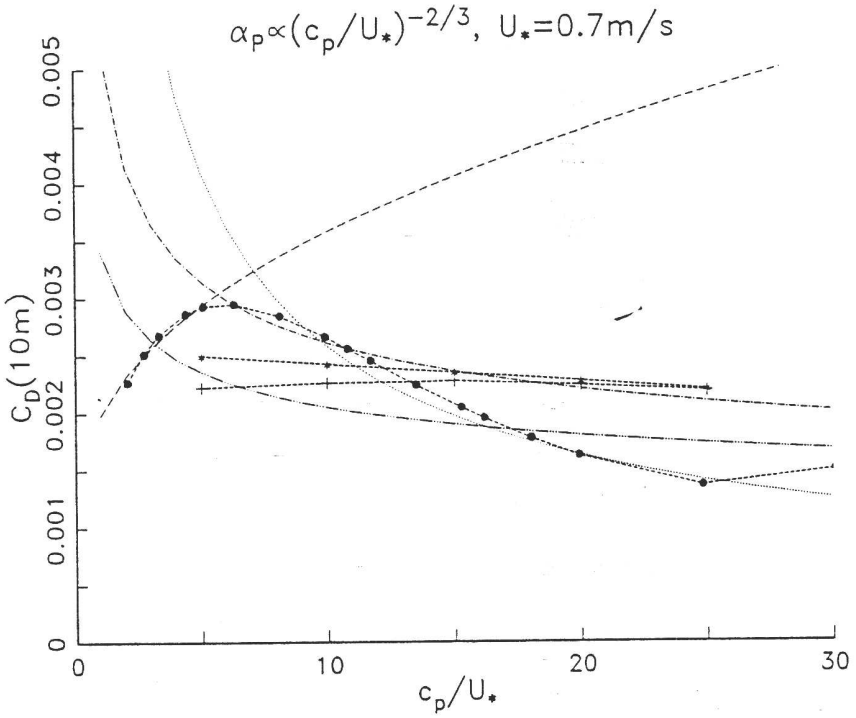

FIG. 18. Drag coefficient for $z = 10$ m with Phillips parameter $\alpha_P = 0.054(c_p/U_*)^{-2/3}$ and friction velocity $U_* = 0.7$ m s^{-1}. Close dashed lines (short dashes): model results—with solid circles, present model; with asterisks, Janssen (1989); with plus signs, Jenkins (1992). Dotted line: curve fitted by Geernaert et al. (1987) to field experimental results with a range of values of U_*. Close dashed line (long dashes): from the relation of Toba and colleagues [Toba and Koga 1986, Eqs. (9) and (10)]. Dash-dotted line: from HEXMAX measurements (Maat et al. 1991). Dash-and-three-dots line: from Lake Ontario measurements (Donelan 1990).

age, but is inconsistent with other field measurements, and the simplified model predicts that C_D(10 m) reaches a maximum and then decreases. If we refer to Fig. 14 of Toba et al. (1990), on which their relation between roughness length or drag coefficient and wave age can be plotted as a straight line, we see that there are two distinct clusters of points: one cluster corresponding to field measurements with moderate to large wave ages, and the other corresponding to laboratory measurements with very small wave ages. It would be just as plausible to draw a curved line through the clusters, so that the roughness length becomes small for both young and old wind seas. It has also been suggested that laboratory experiments are unreliable predictors of the behavior of the atmospheric boundary layer under field conditions—Donelan (1990), for example, found a relation between roughness length, wave energy, and wave age for laboratory data given by $z_0/\langle\eta^2\rangle^{1/2} = 0.205(U_*/c_p)^{2.18}$, which gives significantly smaller roughness than his corresponding relation (44) for field observations.

For more fully developed sea states, C_D(10 m) decreases with wave age if we hold U_* constant, for constant Phillips parameter α_P and for $\alpha_P \propto (c_p/U_*)^{-2/3}$ as well as for $\alpha_P \propto (c_p/U_*)^{-3/2}$. So do the experimentally measured values, though they tend to decrease more slowly. The more computationally expensive models of Janssen (1989) and Jenkins (1992) do appear to predict the field observations better, as do the simple models of Janssen (1991) and Chalikov and Makin (1991), if we assume that $\alpha_P \propto (c_p/U_*)^{-3/2}$. Nordeng's (1991) model, in common with the present model, predicts a maximum in the drag coefficient but for significantly older sea states.

The simplified model's second increase in the drag coefficient, for old wind seas, can be seen prominently in the contour plots of Figs. 12–14. It is a result of the 10-m level moving into the square root part of the wind profile, and has a counterpart in a few data points of Geernaert et al. (1987, Fig. 7), which also show an "upturn," though this may be a coincidence. It is probable that a proportion of the air–sea momentum flux is in fact carried by direct viscous drag on the sea surface [or by a different wind–wave interaction mechanism than that of Miles (1957)], so that $\tau_w < \rho U_*^2$ at $z = 0$. The transition between the "square root" and "logarithmic" behavior should then be more gradual.

An advantage of the present model is that it has only one free, tunable parameter, α_P, which determines the wave spectrum and which in this paper I have assumed

to be a function of c_p/U_*. Although turbulence is neglected in computing the oscillatory components of the airflow, it is taken into account in determining the mean flow, and Figs. 2–3 show plausible mixing length and eddy viscosity profiles. The model cannot be expected to account for momentum flux due to effective roughness contributions other than deep-water gravity wave generation. Unlike the models of Janssen (1989, 1991), Chalikov and Makin (1991), and Jenkins (1992), the present model is able to predict an increase in C_D(10 m) as the wave age is decreased even when α_P is made *constant*, for a rather wide range of U_* and c_p/U_* (see Fig. 12). This behavior is significant, since there is experimental evidence that the variation of α_P with wave age may be rather slow (Banner et al. 1989).

To conclude, the present model, given its simplicity, produces a fairly realistic representation of the behavior of the drag coefficient over wind seas, and may help to resolve some of the difficulties involved in reconciling laboratory and field experimental results. That no "artificial" surface roughness parameter is used, all the air–sea momentum flux being carried by the generation of gravity waves, is an important feature of the model, as the model results then indicate to what extent we can use gravity wave generation to support the momentum flux. The drag coefficient is predicted to be sensitive to the formulation of the Phillips parameter as a function of wave age (or, indeed, of other conditions). Experiments at scales intermediate between those of past laboratory and field studies would provide useful information on the behavior of the drag coefficient for very young wind seas. The model's results for wave generation rates are quite crude: it may be possible to improve them by considering different types of wave spectra and wind velocity profile, at the probable cost of greater computational effort. More general wave spectra, including directional spectra, could also be employed, though the mathematical analysis, and also the computation, would be more complicated.

Acknowledgments. I would like to thank the following people for useful and stimulating discussions: Fred Dobson, Mark Donelan, Peter Janssen, Kristina Katsaros, and Stu Smith. Constructive criticism by two anonymous referees helped to improve the manuscript.

REFERENCES

Al-Zanaidi, M. A., and W. H. Hui, 1984: Turbulent airflow over water waves—A numerical study. *J. Fluid Mech.*, **148**, 225–246.

Banner, M. L., 1990a: The influence of wave breaking on the surface pressure distribution in wind-wave interactions. *J. Fluid Mech.*, **211**, 463–495.

——, 1990b: Equilibrium spectra of wind waves. *J. Phys. Oceanogr.*, **20**, 966–984.

——, I. S. F. Jones, and J. C. Trinder, 1989: Wavenumber spectra of short gravity waves. *J. Fluid Mech.*, **198**, 321–344.

Chalikov, D. V., 1978: The numerical simulation of wind-wave interaction. *J. Fluid Mech.*, **87**, 561–582.

——, 1986a: Spectrum of energy flux to waves. *Oceanology*, **26**, 145–148. [English translation.]

——, 1986b: Numerical simulation of the boundary layer above waves. *Bound.-Layer Meteor.*, **34**, 63–98.

——, and V. K. Makin, 1991: Models of the wave boundary layer. *Bound.-Layer Meteor.*, **56**, 83–99.

——, and M. Yu. Belevich, 1993: One-dimensional theory of the wave boundary layer. *Bound.-Layer Meteor.*, **63**, 65–96.

Charnock, H., 1955: Wind stress on a water surface. *Quart. J. Roy. Meteor. Soc.*, **81**, 639–640.

Conte, S. D., and J. W. Miles, 1959: On the numerical integration of the Orr–Sommerfeld equation. *J. Soc. Ind. Appl. Math.*, **7**, 361–366.

Csanady, G. T., 1985: Air–sea momentum transfer by means of short-crested wavelets. *J. Phys. Oceanogr.*, **15**, 1486–1501.

——, 1990: Momentum flux in breaking wavelets. *J. Geophys. Res.*, **95**(C8), 13 289–13 299.

Donelan, M., 1982: The dependence of the aerodynamic drag coefficient on wave parameters. *Proc. First Int. Conf. on Meteorology and Air–Sea Interaction of the Coastal Zone*, The Hague, Amer. Meteor. Soc., 381–387.

——, 1990: Air–sea interaction. *The Sea*, Vol. 9, B. LeMehaute and D. Hines, Eds., Wiley, 239–292.

Fabrikant, A. L., 1976: Quasilinear theory of wind-wave generation. *Izv. Acad. Sci. USSR, Atmos. Oceanic Phys.*, **12**, 524–526. [English translation.]

Garratt, J. R., 1977: Review of drag coefficients over oceans and continents. *Mon. Wea. Rev.*, **105**, 915–929.

Geernaert, G. L., S. E. Larsen, and F. Hansen, 1987: Measurements of the wind stress, heat flux, and turbulence intensity during storm conditions over the North Sea. *J. Geophys. Res.*, **92**(C12), 13 127–13 139.

Glazman, R. E., 1986: Statistical characterization of sea surface geometry for a wave slope field discontinuous in the mean square. *J. Geophys. Res.*, **91**(C5), 6629–6641.

——, and P. B. Weichman, 1989: Statistical geometry of a small surface patch in a developed sea. *J. Geophys. Res.*, **94**(C4), 4998–5010.

Hasselmann, K., T. P. Barnett, E. Bouws, H. Carlson, D. E. Cartwright, K. Enke, J. A. Ewing, H. Gienapp, D. E. Hasselmann, P. Kruseman, A. Meerburg, P. Müller, D. J. Olbers, K. Richter, W. Sell, and H. Walden, 1973: Measurements of wind-wave growth and swell decay during the Joint North Sea Wave Project (JONSWAP). *Dtsch. Hydrogr. Z.*, **A8**(Suppl.), No. 12, 1–95.

Hasselmann, S., K. Hasselmann, J. H. Allender, and T. P. Barnett, 1985: Computations and parameterizations of the nonlinear energy transfer in a gravity-wave spectrum. Part II: Parameterizations of the nonlinear energy transfer for application in wave models. *J. Phys. Oceanogr.*, **15**, 1378–1391.

Hsu, C.-T., H.-Y. Wu, E.-Y. Hsu, and R. L. Street, 1982: Momentum and energy transfer in wind generation of waves. *J. Phys. Oceanogr.*, **12**, 929–951.

Janssen, P. A. E. M., 1982: Quasilinear approximation for the spectrum of wind-generated water waves. *J. Fluid Mech.*, **117**, 493–506.

——, 1989: Wave-induced stress and the drag of air flow over sea waves. *J. Phys. Oceanogr.*, **19**, 745–754.

——, 1991: Quasi-linear theory of wind-wave generation applied to wave forecasting. *J. Phys. Oceanogr.*, **21**, 1631–1642.

——, P. Lionello, and L. Zambresky, 1989: On the interaction of wind and waves. *Phil. Trans. Roy. Soc. London*, **A329**, 289–301.

Jeffreys, H., 1925: On the formation of water waves by wind. *Proc. Roy. Soc. London*, **A107**, 189–206.

Jenkins, A. D., 1992: A quasi-linear eddy viscosity model for the flux of energy and momentum to wind waves, using conservation-law equations in a curvilinear coordinate system. *J. Phys. Oceanogr.*, **22**, 843–858.

Kawai, S., 1981: Visualization of airflow separation over wind-wave crests under moderate wind. *Bound.-Layer Meteor.*, **21**, 93–104.

——, 1982: Structure of air flow separation over wind wave crests. *Bound.-Layer Meteor.*, **23**, 503–521.
Kitaigorodskii, S. A., 1973: *The Physics of Air–Sea Interaction.* Israel Program for Scientific Translations, 237 pp. [English translation.]
Landau, L., 1946: On the vibrations of the electronic plasma. *J. Phys. (U.S.S.R.)*, **10**, 25.
Lin, C. C., 1955: *The Theory of Hydrodynamic Stability,* Cambridge University Press, 155 pp.
Maat, N., and V. K. Makin, 1992: Numerical simulation of air flow over breaking waves. *Bound.-Layer Meteor.*, **60**, 77–93.
——, C. Kraan, and W. A. Oost, 1991: The roughness of wind waves. *Bound.-Layer Meteor.*, **54**, 89–103.
Makin, V. K., 1980: Numerical simulation of the structure of the near water atmospheric layer in the presence of a developed sea. *Oceanology,* **20**, 139–142. [English translation.]
——, 1982: Numerical studies of wind-wave interaction. *Oceanology,* **22**, 525–530. [English translation.]
——, 1987: Wavelike momentum fluxes in boundary layer above sea waves. *Oceanology,* **27**, 128–132. [English translation.]
——, and Ye. G. Panchenko, 1986: Numerical studies of energy transfer from the wind to wind waves along a limited fetch. *Izv. Acad. Sci. USSR, Atmos. Oceanic Phys.*, **22**, 163–165. [English translation.]
Mandelbrot, B. B., 1983: *The Fractal Geometry of Nature.* Freeman, 468 pp.
Miles, J. W., 1957: On the generation of surface waves by shear flows. *J. Fluid Mech.*, **3**, 185–204.
Nordeng, T. E., 1991: On the wave age dependent drag coefficient and roughness length at sea. *J. Geophys. Res.*, **96**(C4), 7167–7174.
Okuda, K., S. Kawai, and Y. Toba, 1977: Measurement of skin friction distribution along the surface of wind waves. *J. Oceanogr. Soc. Japan,* **33**, 190–198.
Phillips, O. M., 1958: The equilibrium range in the spectrum of wind-generated waves. *J. Fluid Mech.*, **4**, 426–434.
——, 1985: Spectral and statistical properties of the equilibrium range in wind-generated gravity waves. *J. Fluid Mech.*, **156**, 505–531.
Pierson, W. J., and L. Moskowitz, 1964: A proposed spectral form for fully developed wind seas based on the similarity theory of S. A. Kitaigorodskii. *J. Geophys. Res.*, **69**, 5181–5190 and 5202.
Plant, W. J., 1982: A relationship between wind stress and wave slope. *J. Geophys. Res.*, **87**(C3), 1961–1967.
Prandtl, L., 1925: Bericht über Untersuchungen zur ausgebildeten Turbulenz. *Z. angew. Math. Mech.*, **5**, 136–139.
Schlichting, H., 1968: *Boundary Layer Theory,* 6th ed. McGraw-Hill, 747 pp.
Snyder, R. L., F. W. Dobson, J. A. Elliott, and R. B. Long, 1981: Array measurements of atmospheric pressure fluctuations above surface gravity waves. *J. Fluid Mech.*, **102**, 1–59.
Stewart, R. W., 1961: The wave drag of wind over water. *J. Fluid Mech.*, **10**, 189–194.
——, 1974: The air–sea momentum exchange. *Bound.-Layer Meteor.*, **6**, 151–167.
Toba, Y., 1979: Study on wind waves as a strongly nonlinear phenomenon. *Twelfth Symp. on Naval Hydrodynamics,* Natl. Acad. Sci., Washington, D.C. 529–540.
——, and M. Koga, 1986: A parameter describing overall conditions of wave breaking, white-capping, sea-spray production and wind stress. *Oceanic Whitecaps,* E. C. Monahan and G. Mac Niocaill, Eds., D. Reidel, 37–47.
——, N. Iida, H. Kawamura, N. Ebuchi, and I. S. F. Jones, 1990: Wave dependence of sea-surface wind stress. *J. Phys. Oceanogr.*, **20**, 705–721.
Tollmien, W., 1931: The production of turbulence. National Advisory Committee for Aeronautics Tech. Memo., No. 609, Washington, D.C., 32 pp. [English translation.]
Wu, J., 1980: Wind-stress coefficients over sea surface near neutral conditions—A revisit. *J. Phys. Oceanogr.*, **10**, 727–740.
——, 1986: Roughness elements of the sea surface—Their spectral composition. *Tellus,* **38A**, 178–188.
——, E.-Y. Hsu, and R. L. Street, 1979: Experimental study of nonlinear wave–wave interaction and white-cap dissipation of wind-generated waves. *Dyn. Atmos. Oceans,* **3**, 55–78.
Yuen, H. C., and B. M. Lake, 1979: A new model for nonlinear wind waves. Part 2. Theoretical model. *Stud. Appl. Math.*, **60**, 261–270.